Phase Transitions

A Multinational Journal

ISSN: 0141-1594 (Print) 1029-0338 (Online) Journal homepage: www.tandfonline.com/journals/gpht20

Frequency and temperature dependent dielectric behavior of NiCr2O4 spinels synthesized via sol-gel route – Effect of sintering temperature

Katrapally Vijaya Kumar, Rajesh Siripuram, Panthagani Raju, Madireddy Buchi Suresh & Jhuma Biswas

To cite this article: Katrapally Vijaya Kumar, Rajesh Siripuram, Panthagani Raju, Madireddy Buchi Suresh & Jhuma Biswas (22 Aug 2025): Frequency and temperature dependent dielectric behavior of NiCr2O4 spinels synthesized via sol-gel route – Effect of sintering temperature, Phase Transitions, DOI: 10.1080/01411594.2025.2548866

To link to this article: https://doi.org/10.1080/01411594.2025.2548866

PHASE TRANSITIONS
https://doi.org/10.1080/01411594.2025.2548866

Frequency and temperature dependent dielectric behavior of NiCr2O4 spinels synthesized via sol-gel route – Effect of sintering temperature

Katrapally Vijaya Kumar[a], Rajesh Siripuram[b], Panthagani Raju[c], Madireddy Buchi Suresh[d] and Jhuma Biswas[e]

[a]Department of Physics, JNTUH University College of Engineering Sultanpur, Sangareddy-District, Telangana, India; [b]Department of Physics, JNTUH University College of Engineering Jagtial, Jagtial-District, Telangana, India; [c]Department of Freshman Engineering, Geethanjali College of Engineering and Technology, Hyderabad, Telangana, India; [d]International Advanced Research Institute for Powder Metallurgy and Material Processing (ARCI), Hyderabad, Telangana, India; [e]Department of Physics, Pandu College, Guwahati, Assam, India

ABSTRACT

Nickel chromite spinel, represented by the chemical formula $NiCr_2O_4$, were synthesized through the sol–gel (auto-combustion) method. The samples were subsequently subjected to sintering at temperatures of 700, 900, 1100, and 1300°C. The XRD data analyzed at room temperature employed the Rietveld refinement method to ascertain the material's phase. The dielectric constant, loss tangent, and AC conductivity were measured using an LCR meter at room temperature and across a temperature range of 100 to 800°C, at frequencies ranging from 100 Hz to 10 MHz. The plots of the dielectric constant ε' against frequency indicate that the dielectric characteristics of $NiCr_2O_4$ spinel are representative of expected behavior. The dielectric loss variance (ε'') for each sample exhibits a decreasing trend with respect to frequency. The Nyquist plot demonstrates the occurrence of phenomena like grain and grain boundaries at specific temperatures. The evidence of Maxwell–Wagner interfacial polarization significantly strengthened the findings. With increasing frequency and temperature in the range of 100°C to 800°C, a significant reduction in the dielectric properties is observed.

ARTICLE HISTORY
Received 15 April 2025
Accepted 13 August 2025

KEYWORDS
$NiCr_2O_4$ spinel; dielectric constant; loss tangent; impedance; Cole-Cole plots; AC conductivity

1. Introduction

Spinel oxides, defined by the formula AB_2O_4, exhibit complex phase diagrams due to the interconnections among their structural, electrical, and magnetic properties. The chromite spinel ACr_2O_4, where A includes Mn^{2+}, Fe^{2+}, Co^{2+}, Ni^{2+}, Cu^{2+}, among others, have attracted considerable research interest. The increased interest is due to their intricate spin configuration, which leads to a variety of properties such as ferroelectric polarization, magneto-dielectric effects, magneto-elastic behavior, and the development of magnetoelectric multiferroic characteristics [1–4]. Chromite spinel generally exhibit a normal cubic spinel structure, defined by the Fd3 m space group. A^{2+} ions are organized in a diamond lattice, exhibiting tetrahedral coordination with oxygen ions. Cr^{3+} ions concurrently establish a pyrochlore lattice in an octahedral oxygen environment. Crystal symmetry reduction occurs as a result of the Jahn–Teller effect when A is Ni, Fe, or Cu, which exhibit orbital and spin degeneracy [5–7]. The interaction between A site and frustrated Cr site magnetism in ACr_2O_4 leads to spin-driven symmetry reduction and the emergence of spiral magnetic order.

CONTACT Katrapally Vijaya Kumar kvkphd@gmail.com

This article has been corrected with minor changes. These changes do not impact the academic content of the article.

The strong correlations among spin, lattice, and orbital degrees of freedom contribute to the intriguing magnetic, dielectric, and multiferroic properties observed in ACr_2O_4 [8–10]. Multiferroic materials, which integrate electrical and magnetic properties, are crucial for advancing multifunctional devices and enhancing the understanding of their fundamental physics. While these features have been documented in several spinel chromites [3,11–14], the majority of research emphasizes properties at temperatures significantly below room temperature (RT), particularly facing challenges in attaining RT magnetism. From a technological perspective, the main objective in this area is to create new chromite-based single-phase materials that exhibit improved magnetic and dielectric properties close to room temperature. This investigation entails a comprehensive analysis of the structural, magnetic, frequency and temperature-dependent dielectric properties of polycrystalline $NiCr_2O_4$. As a standard spinel oxide, $NiCr_2O_4$ has a cubic crystalline structure with the Fd3 m space group above room temperature ($T > 310$ K). The Jahn–Teller distortion (JTD) is crucial for lifting orbital degeneracy in the t_{2g} orbitals of Ni^{2+} ($e_g^4\, t^4{}_{2g}$) ions located in tetrahedral sites. The distortion leads to a structural transition from cubic to tetragonal, characterized by the I41/amd space group, occurring at approximately 310 K [6,15,16]. Nonetheless, various research teams have reported conflicting findings concerning smaller crystallite sizes [17–19]. Furthermore, the dielectric characteristics, encompassing the real (ε') and imaginary (ε'') aspects of complex permittivity, are highlighted in numerous applications of electronic materials. The real component (ε') signifies material polarizability, while the imaginary component (ε'') reflects energy dissipation due to polarization and ionic conduction. The structure, composition, and fabrication technique of a material significantly affect its permittivity, serving as an indicator of molecular relaxation and transport phenomena. In the realm of wireless communication, there is a notable trend towards materials that exhibit high dielectric constants coupled with low dielectric losses. Materials with a high dielectric constant, such as metal-doped ceramics, find extensive application in field emission devices, gas sensors, solar cells, catalysis, and biological applications [20–22]. A comprehensive discussion on multiferroics, grounded in experimental data for a single $NiCr_2O_4$, remains to be finalized. The necessary physical mechanism for the coexistence or correlation of magnetic and electric properties is lacking in $NiCr_2O_4$. This study presents the effect of temperature and frequency on dielectric, impedance and conductivity properties of polycrystalline $NiCr_2O_4$ spinels sintered at 700, 900, 1100, 1300°C in detail at ambient temperature and across a broad temperature spectrum of 100–800°C. Furthermore, an attempt has been made to explore the effect of temperature on dielectric and impedance properties of $NiCr_2O_4$ spinels at specific frequencies. The ε' (dielectric constant) dielectric loss (ε'') exhibits deterioration significantly at room temperature, adversely, both parameters increase over the temperature range of 100-800°C. As evidenced by experimental observations, the real, imaginary impedances and AC conductivities shows dependence of both frequency and temperature. The high dielectric constant, low dielectric loss tangent and lower AC conductivity of prepared samples makes them as a potential candidate for multifunctional devices.

2. Experimental

Nickel chromites were produced through the sol–gel auto-combustion method. The reactants, nickel nitrate and chromium oxide, were combined in a stoichiometric ratio within an aqueous solution. Subsequently, a 1:3 ratio of citric acid was incorporated into the nitrate solution. The utilization of ammonia maintains the pH at a neutral level of seven. The liquid was subsequently combined and heated to 100°C to form a viscous gel. The gel formation commenced with an increase in temperature to 200°C. The dry gel underwent complete ignition, transforming into a loose powder through a self-sustaining combustion process. Following further synthesis, the powder underwent sintering for eight hours at various temperatures of 700, 900, 1100, and 1300°C. Phillips X'pert diffractometer has been employed to study the crystalline nature of synthesized nickel chromites at room temperature, covering the 20° to 80° range. Rietveld refinement was conducted

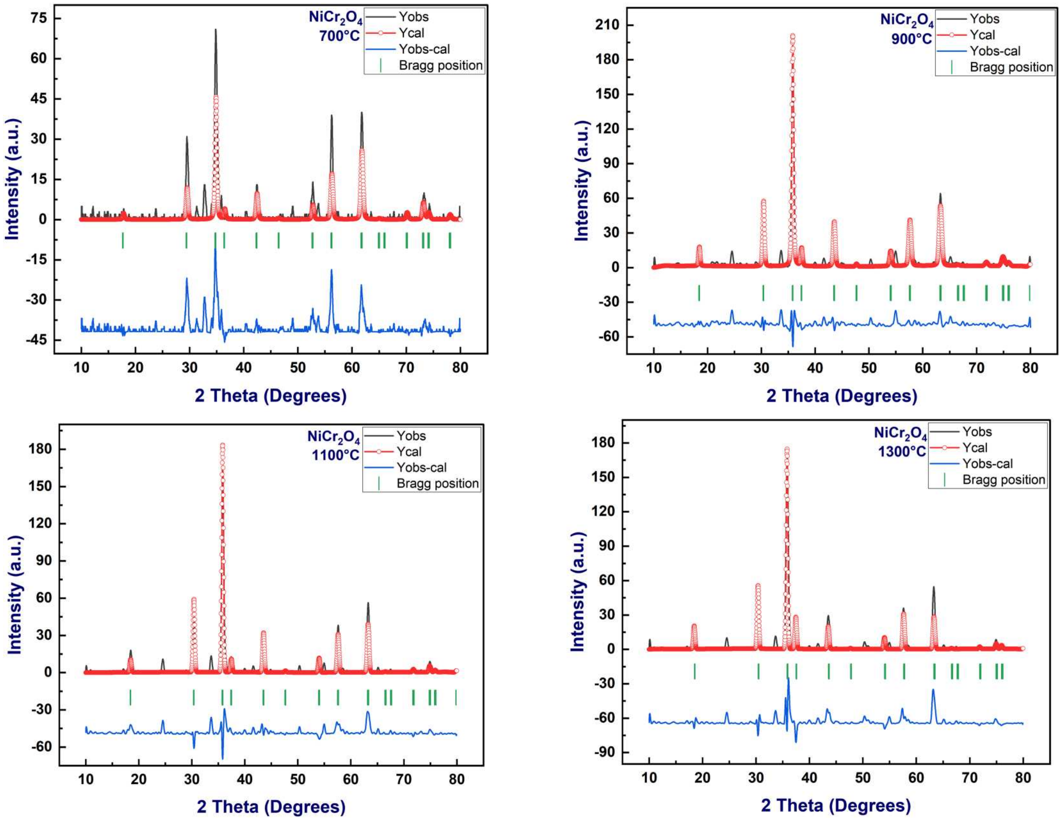

Figure 1. Rietveld refinement plots of nickel chromite calcinated at 700, 900, 1100 and 1300°C.

to verify the phase of the produced nickel chromites. The powders, measuring 11 mm in diameter and 1.5 mm in thickness, were subjected to a pressure of 0.5 tons and subsequently compressed into pellets. An LCR meter was employed to assess the dielectric properties, like ε′ (dielectric constant), ε″ (dielectric loss), and loss tangent (tanδ), over frequencies and temperatures ranging from 100 Hz to 10 MHz, 100 to 800 °C. The equation $\varepsilon' = C \times t/\varepsilon_0 \times A$, with C representing capacitance, t indicating thickness, A denoting the pellet's cross-sectional area, and ε_0 symbolizing the permittivity of free space, was employed to determine the ε′ of the produced pellets. The time varying current of prepared chromites was determined using the equation $\sigma_{AC} = \varepsilon\varepsilon_0\omega \mathrm{Tan}\delta$, where the angular frequency is expressed as $\omega = 2\pi f$. Tanδ equals ε″ divided by ε′. The samples' impedance was assessed over a temperature range of 100 to 800°C and frequency spectrum of 100 Hz to 10 MHz [23].

3. Results and discussions

3.1. X-ray diffraction analysis

The X-ray powder diffraction patterns of the samples sintered for 8 hours at 700, 900, 1100, and 1300°C temperatures are presented in Figure 1. All patterns distinctly exhibit the spinel structure characteristic of the cubic phase [24]. Larger Ni^{2+} ions at tetrahedral sites (8a) in regular spinel orientation partially reciprocate positions with octahedral sites, while smaller Cr^{3+} ions are found in octahedral sites in inverse spinel alignment. The standard formula is $\{Cr_x^{3+}\}_{tetra}\ \{Ni^{2+}Cr_{1-x}^{3+}\}_{octa}O_4^{2-}$, with inversion parameter disorder (x) ($0 \le x \le 1$). The distinct peaks observed in the X-ray diffraction patterns elucidated the phase evolution and crystal structure

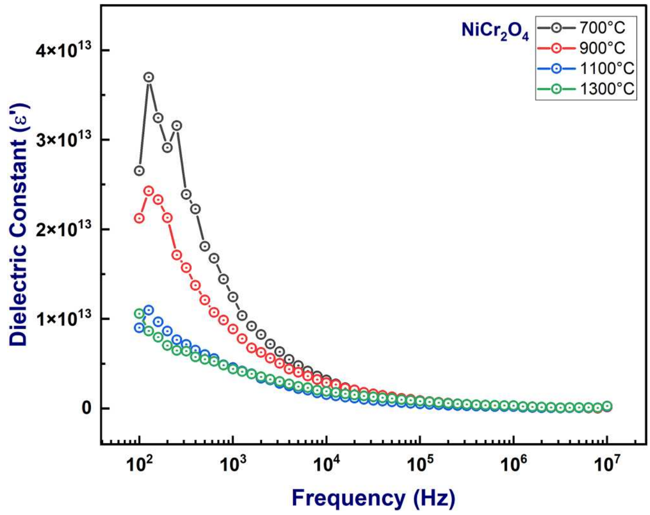

Figure 2. Variation of dielectric constant of nickel chromite calcinated at 700, 900, 1100 and 1300°C with frequency at room temperature.

effectively. Upon comparison with the JCPDS file (File no. 01-088-0109), it is evident that each peak of XRD pattern aligns perfectly with documented results. The peaks were categorized according to the specified patterns. Rietveld refinement was conducted to verify the development of the spinel phase. Figure 1 illustrates a significant correlation between the theoretical predictions and the empirical findings concerning peak position and intensity. The XRD examination has facilitated the determination of the average grain size, average interplanar spacing, and average crystallite size. A different source offers an in-depth analysis of the effect of sintering temperature on size of the grain and crystallite [25].

3.2. Dielectric properties

The frequency dependent dielectric constant (ε′) at ambient temperature for all nickel chromite that was sintered at 700, 900, 1100, and 1300°C is shown in Figure 2. According to the Figure 2, ε′ is higher for all samples in the low-frequency range. Additionally, as higher frequencies increased charge carrier mobility and lowered ε′, the dielectric constant got smaller. In addition, the relaxation process causes the electric dipoles to lag behind the field, which is consistent with Koops' phenomenological view [26–29]. An explanation for this occurrence could be Maxwell–Wagner interfacial polarization. Polarization decreases with increasing electric field frequency because the electrical interaction between Cr^{2+} and Cr^{3+} is insensitive to time-varying fields above a certain frequency. The octahedral [B] site is where Ni^{2+} ions are found in the majority in the present $NiCr_2O_4$ samples, while the tetrahedral (A) site is where Cr^{3+} ions are found. The octahedral [B] site facilitates the exchange interaction that follows:

$$Cr^3 + +Ni^2+ \Leftrightarrow Ni^3 + +Cr^2+$$

While electron hopping from Cr^{2+} to Cr^{3+} is the primary conduction process in n-type semiconductors, electron transfer from Ni^{3+} to Ni^{2+} is the primary mechanism in p-type semiconductors [30]. In this process, polarization is produced by the spatial displacement of electrons in the direction of the projected electric field. They show a similar pattern to ambient temperature dielectric properties. Dielectric permittivity (ε′) is high at low frequencies and decreases with increase in frequency; ions do not react appropriately and instead gather in areas where the applied field is

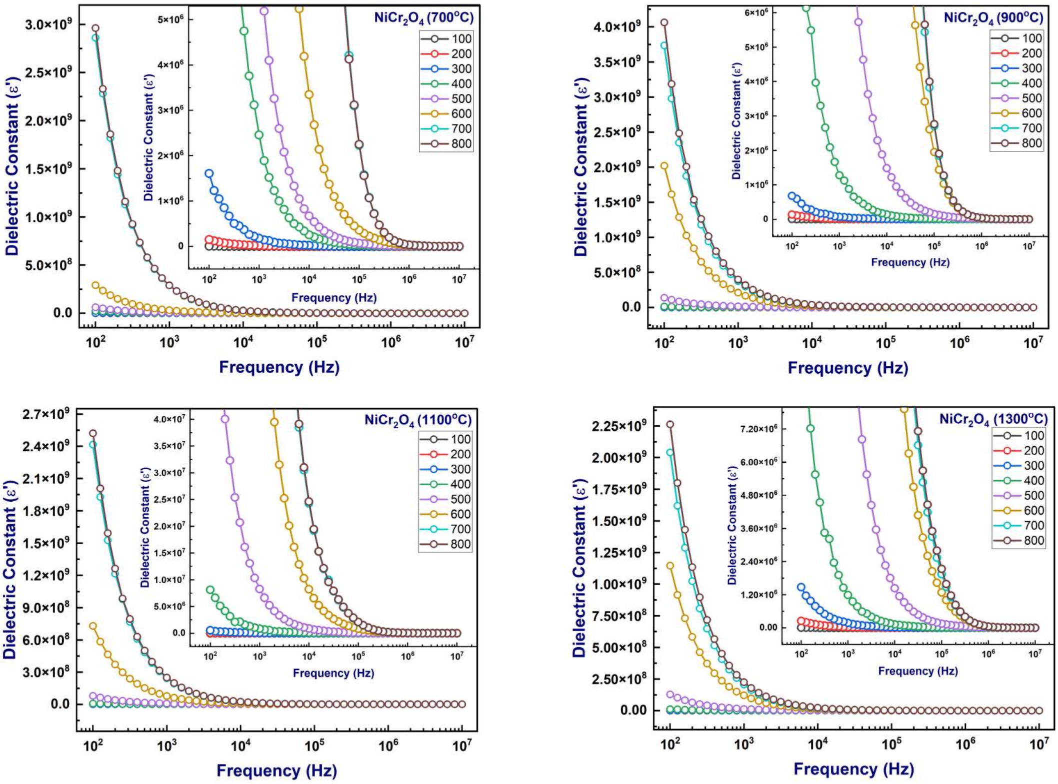

Figure 3. Variation of dielectric constant of nickel chromite calcinated at 700, 900, 1100 and 1300°C with frequency in the temperature range 100-800°C.

opposed by large free energy barriers. Since charge accumulation at the grain boundary causes a net polarization effect, the dielectric constant (ε′) increases at lower frequencies [31]. A dipole moment that resists conforming to the applied field, especially at high frequencies, is a comparable representation of a minimal dielectric permittivity. It is claimed that when the frequency increases, the dielectric constant (ε′) decreases. Muhammad Younis *et.al* reported that this behavior aligns with Koop's theory [32] and is supported by the Maxwell interfacial polarization model. The chromite materials are thought to consist of two layers within the grains and grain boundaries, which play a crucial role in the development of the dielectric structure in chromites. The presence of a pure crystalline phase results in reduced electrical resistance, as the grains exhibit fewer defects. However, the resistance increases due to the greater defects found at the grain boundaries. Charges are accumulated at grain boundary sides due to high resistance which results Maxwell – Wagner's type of interfacial polarization. Numerous materials exhibit this characteristic, and applications like radio frequency and microwave communications require a particular understanding of how the dielectric constant value varies with increasing frequency. However, the dielectric constant falls as the calcination temperature rises. This may be because the material gets denser and the crystals inside it form better as the calcination temperature rises [33]. Figure 3 shows how the dielectric constant varies with temperature for every nickel chromite that was sintered at 700, 900, 1100, and 1300°C. The magnitude of ε′ showed a direct increase with temperature at a particular frequency. This behavior could be explained by dipoles not aligning with the field direction at low temperatures. But when the temperature rose, the dipoles gained enough energy, and the thermal motions made it easier for them to line up with the field's direction. The dielectric constant's magnitude increased in tandem with the temperature. A thorough analysis of temperature dependent dielectric

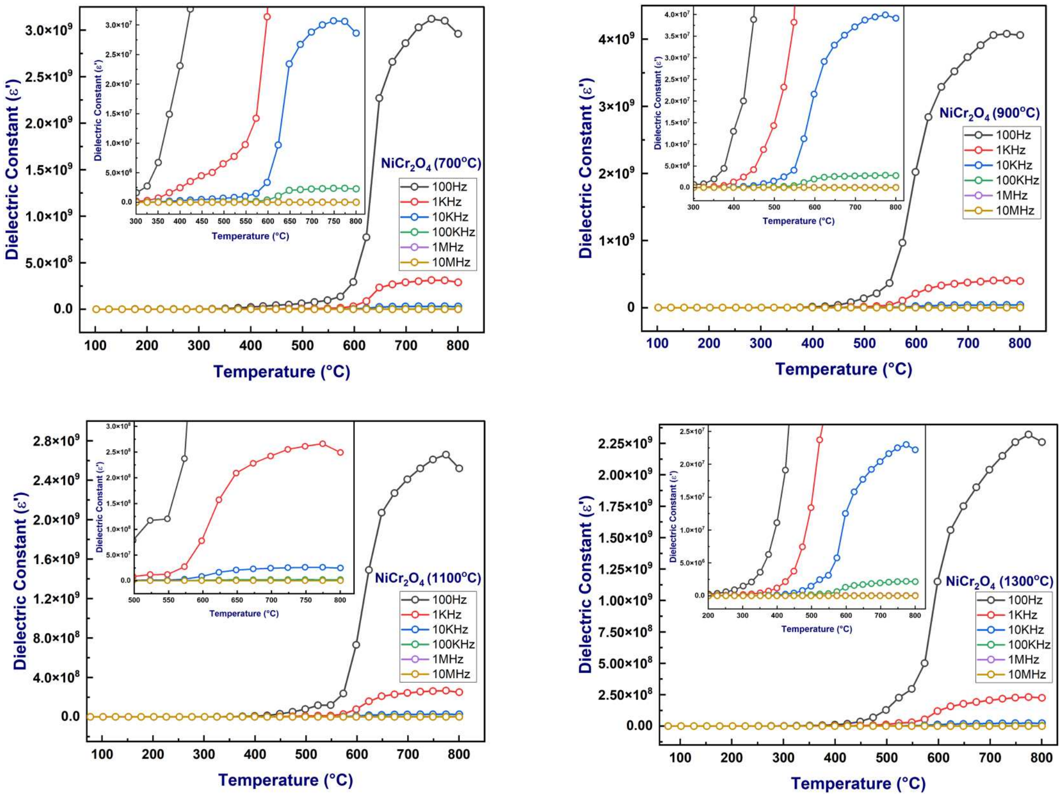

Figure 4. Variation of dielectric constant of nickel chromite calcinated at 700, 900, 1100 and 1300°C with temperature at 100 Hz, 1kHz, 10kHz, 100kHz, 1 and 10 MHz.

constant at selected frequencies is shown in Figure 4. The dielectric constant rises with increasing temperature but decreases with increasing frequency. Additionally, it is shown that the dielectric constant exhibits two discrete plateaus at various temperatures, indicating a clear relationship with relaxation behavior [34–36]. Nevertheless, the dielectric permittivity reaches enormous values, approximately 10^9. An extrinsic effect, the large capacitance of the grain boundaries, is linked to the enormous dielectric response in the current samples [37]. For all frequencies, the dielectric constant behaves reasonably consistently up to 550°C. The dielectric constant progressively rises over 550°C, with a broad peak appearing about Neel temperature (T_N). A property common to relaxer ferroelectrics is that this broad peak near T_N is frequency dependent. The peak shifting to a higher temperature and decreasing in strength with increasing frequency which could be due to magnetoelectric coupling directly causes this kind of dielectric anomaly [38,39]. Further, In the low temperature range the electric field and an increase in the number of charge carriers (electrons) both increase polarization; as a result, the dielectric constant (ε') rises as a result of both temperature and frequency increases. The production of charge carriers reaches saturation for the high temperature range. As a result, the dielectric constant falls because the electron exchange between ions of the same element that are present in many valence states (Ni^{+2}, Ni^{+1}) cannot follow the field variation. [40] The dielectric loss (ε'') fluctuation for nickel chromite sintered at 700, 900, 1100, and 1300°C as a function of log(f) at room temperature is shown in Figure 5. The dielectric behavior of each sintered sample is distinctive. According to the investigation, ε'' decreases exponentially with increasing frequency for all substances analysed, and its magnitude decreases with rising sintering temperatures. Grain boundary defects and an increase in oxygen vacancies are the main causes of the decrease in dielectric loss seen in Figure 5 as frequency rises. Furthermore, the charge

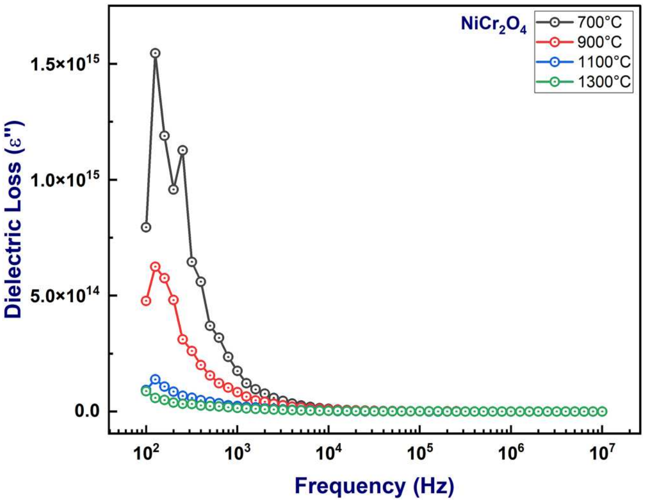

Figure 5. Variation of dielectric loss of nickel chromite calcinated at 700, 900, 1100 and 1300°C with frequency at room temperature.

carriers cannot follow the trajectory of high-frequency waves. Dipoles have enough time to adequately align at lower frequencies with the applied field. As a result, the main cause of dielectric loss will be internal friction [39]. The frequency dependent of ε″ at various temperatures is depicted in Figure 6. Das. L. *et.al* [41] reported that, dielectric loss rises with temperature, primarily because of increased charge carrier mobility, which causes more polarization and more dielectric loss. At high temperatures, substantial dielectric loss is caused by charge build-up at grain boundaries. In smaller particles, a higher surface area-to-volume ratio raises the possibility of surface charges building up, accounting for the contribution of surface charge polarization. As the calcination temperature rises, a greater surface charge polarization is produced, which results in larger crystal sizes and a lower surface charge polarization. As a result, dielectric loss decreases as the calcination temperature rises. Figure 7 shows the temperature dependency of the dielectric loss tangent at specific frequencies. An electromagnetic wave's energy loss in the medium as it travels through it is measured by dielectric loss (tanδ). In addition to measuring the dissipation of electric field energy, it calculates the ability to support the electric field. For materials sintered at 700, 900, 1100, and 1300°C, tanδ shows a parabolic pattern around 650°C as shown in Figure 7. As the temperature rises, the tanδ values also rise. The free migration of charge, space charge polarization, and material defects are the causes of the high-temperature region's sharp rise [42]. A noticeable peak in the dielectric loss tangent indicates that there is a spread of relaxation durations rather than a single value. Further, as frequency increases from 100 Hz to 10 MHz, the peak value of tanδ shifts towards lower temperatures [43]. Increased ac electrical conductivities are the result of thermally activated electrons' increased drift mobility with temperature. Therefore, an increase in dielectric polarization results in an increase in tanδ [44]. In contrast, [45] the dielectric loss variation with temperature shows the same characteristics as the dielectric constant (ε') fluctuation with temperature and can be described using the same methodology as the dielectric constant (ε') discussion. It is discovered that the dielectric loss rises as the temperature climbs. As the temperature rises, charge carrier mobility rises as well, increasing polarization and dielectric loss. Charge accumulating at grain boundaries is the cause of the increased dielectric loss value that is seen at high temperatures. According to S. K. Mandal *et al.*, the tan (δ) value of NiFe$_2$O$_4$ nanoparticles increases as Ni doping increases. This suggests that as the system's Ni concentration rises, the leakage current increases as well [46].

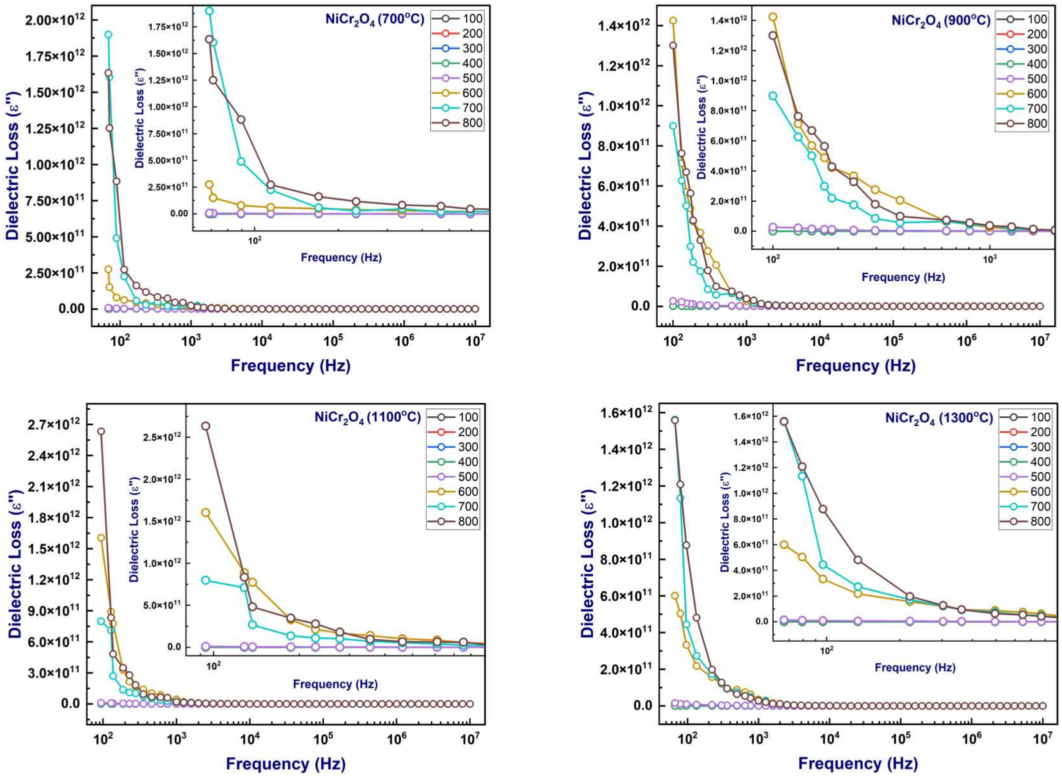

Figure 6. Variation of dielectric loss of nickel chromite calcinated at 700, 900, 1100 and 1300°C with frequency in the temperature range 100-800°C.

A variety of elements, including microstructure, finely separated grains, grain boundaries, electrode interfaces, and inter-regional features, influence the electrical properties of magneto ceramic polycrystalline oxides. The electrical characteristics of nickel chromite were examined through impedance spectra, utilizing an LCR impedance meter between a temperatures and frequency of 100°C to 800°C, 100 Hz to 10 MHz. The real (Z') and imaginary (Z″) components of impedance, along with those of the grain interior and boundary, can be precisely assessed utilizing the EIS methodology [47]. Figure 8 illustrates the variation of Z′ as function of frequency at RT for samples that were sintered at temperatures of 700, 900, 1100, and 1300°C. In each sample, Z' reaches its maximum at lower applied field frequencies before declining as the frequency increases, likely due to the release of space charges [48]. The magnitude of the Z′ rises from 1.6×10^5 to 5.6×10^5 Ohm as the sintering temperature escalates from 700°C to 1300°C. An increase in the density of trapped charges and a decrease in charge carrier mobility are the primary causes of this rise in Z′ values [49]. Utilizing the peak maximum value for every sample allows for a decisive determination of the presence of relaxation effects and fluctuations of materials bulk resistance. The peak indicates the frequency of relaxation of the material. At lower frequencies, the impedance of the samples decreases at a slower rate, while at higher frequencies, it diminishes more rapidly. Figure 9 presents the frequency-dependent Z′ in connection with temperature. With reference to Figure 9. as the temperature rises from 100 to 800°C, the value of Z' consistently declines across all the samples, with the highest magnitude observed at 100°C for each sample. The decrease in Z' as frequency increases may be ascribed to the interfacial polarization effects occurring within the material [14,50,51]. The extreme value of Z′ varies between 1.8×10^5 and 5.6×10^5 Ohm as the temperature rises from 100 to 800°C. The compound's semiconductor behavior is confirmed

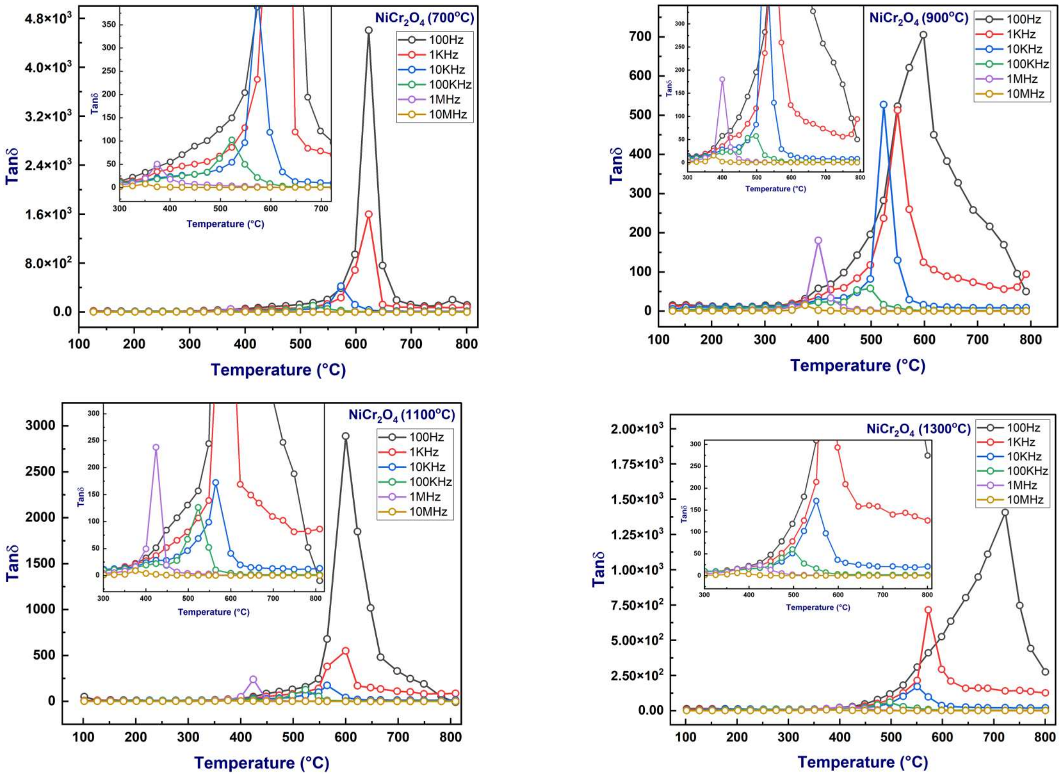

Figure 7. Variation of dielectric loss tangent of nickel chromite calcinated at 700, 900, 1100 and 1300°C with temperature at 100 Hz, 1kHz, 10kHz, 100kHz, 1 and 10 MHz.

by the change in the real component of the impedance with temperature. We identify three inflection points in the curves that correspond to three relaxation phenomena. Interfacial polarization is actually thought to be more important at lower frequencies. Ionic and orientation polarizations, on

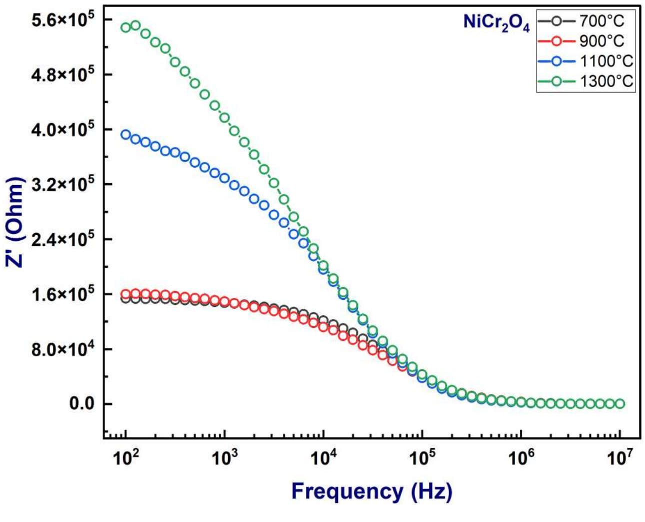

Figure 8. Variation of real part of impedance of nickel chromite calcinated at 700, 900, 1100 and 1300°C with frequency at room temperature.

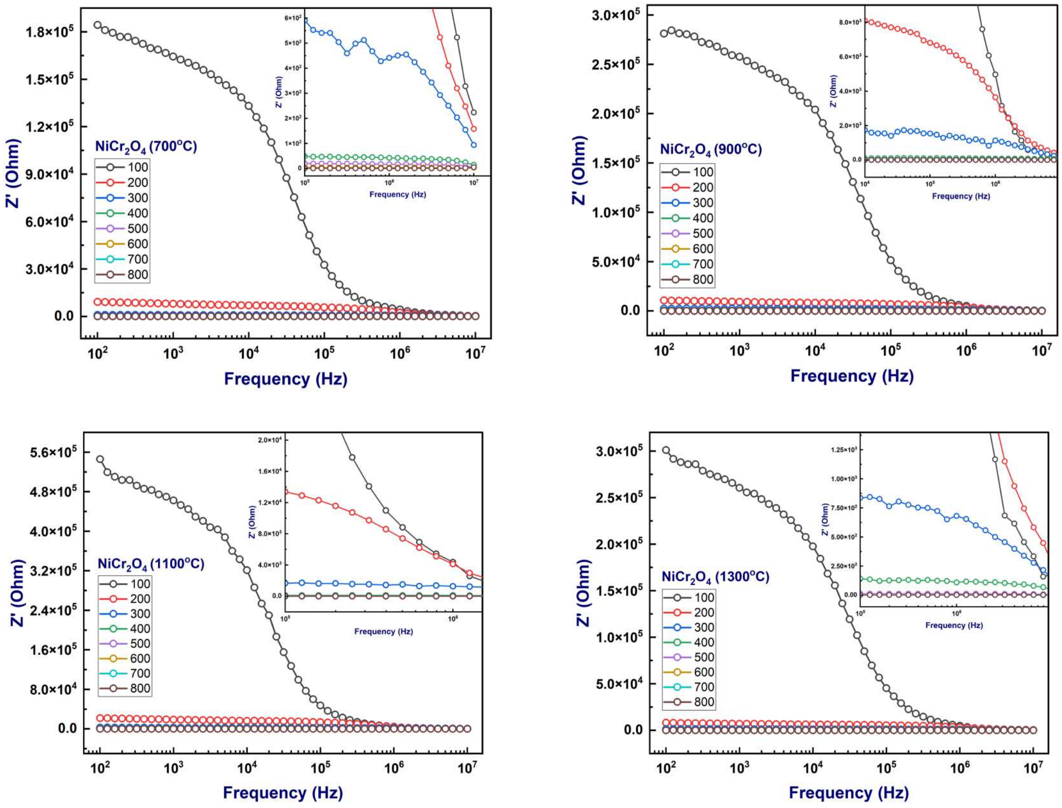

Figure 9. Variation of real part of impedance of nickel chromite calcinated at 700, 900, 1100 and 1300°C with frequency in the temperature range 100-800°C.

the other hand, contribute to the polarization at higher frequencies. The existence of a space-charge area brought on by the decrease in the charge barrier explains the abrupt degradation of impedance. Furthermore, the height of the electron hopping barrier decreased as the temperature rose. This would result in a reduction of the compound's actual obstacles [52]. Figure 10 presents the relationship between Z′ and temperature across selected frequencies ranging from 100 Hz to 10 MHz. It is evident from the figure, the Z′ exhibits a decline with increasing temperature and frequency. The variation of Z″ with frequency at room temperature is seen in Figure 11. Across all sintered samples, the Z″ increases as the applied field frequencies rise, peaks, and then declines with further frequency increases. As the sintering temperature increases, the peak frequency shifts to lower values, indicating a unique relaxing event in the samples. The grain size reduction in nanocrystalline materials results in the appearance of increased dipoles at grain borders. As sintering temperatures increase, the relaxation peak moves to the lower frequency area, which is explained by the significant increase of dipole-to-grained boundary contacts, which lowers the relaxation frequency [53]. As the calcination temperature increases from 700°C to 1300°C, the maximum value of Z″ varies in the range of 6×10^4 Ω to 1.8×10^5Ω with the calcination temperature. The change of Z″ with frequency for nickel chromite at various temperatures is shown in Figure 12. For all sintered materials at 700, 900, 1100, and 1300°C, the samples in this investigation show a single peak, indicating a single relaxation event. In addition to a decrease in peak height and an increase in width with temperature, the peak shifts to higher frequencies as Z″ decreases and temperature rises. The decrease in peak temperature is explained by the disruption caused by frequency within the network, which makes it easier for charge carriers to travel across the CrO$_6$ octahedron. Because of this, Cr and

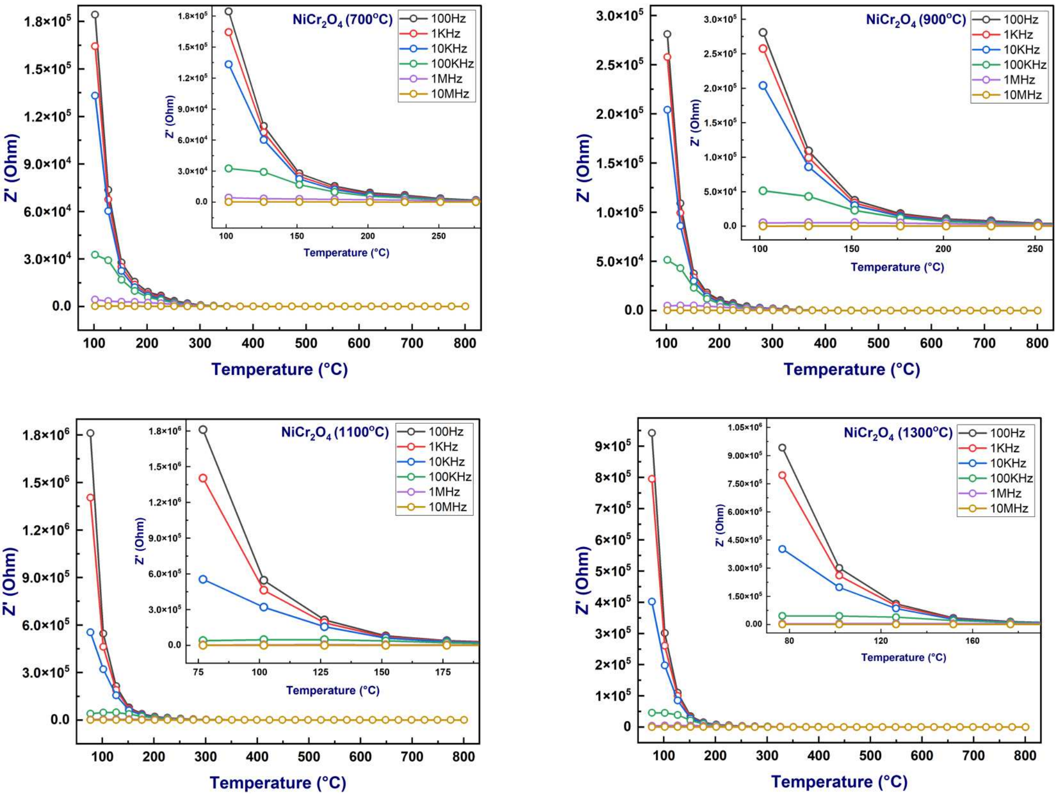

Figure 10. Variation of real part of impedance of nickel chromite calcinated at 700, 900, 1100 and 1300°C with temperature at 100 Hz, 1kHz, 10kHz, 100kHz, 1 and 10 MHz.

O ions oscillate with considerable amplitude, which makes it easier for carriers to be close together and causes site hopping. The frequency facilitates charge carriers' passage over energy barriers, which helps the material relaxation [26]. This behavior suggests the presence of electronic relaxation due to alterations in the bulk resistance of the material, along with the influence of grains and grain boundaries across the structure. An increase in the rate of localized charge carrier

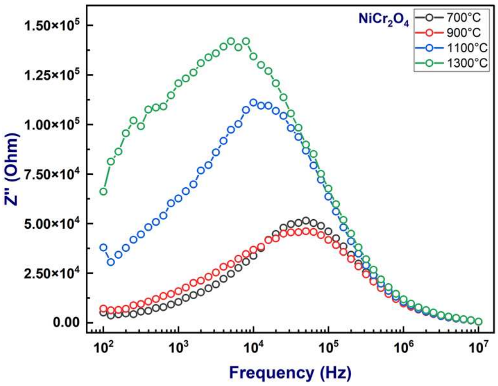

Figure 11. Variation of imaginary part of impedance of nickel chromite calcinated at 700, 900, 1100 and 1300°C with frequency at room temperature.

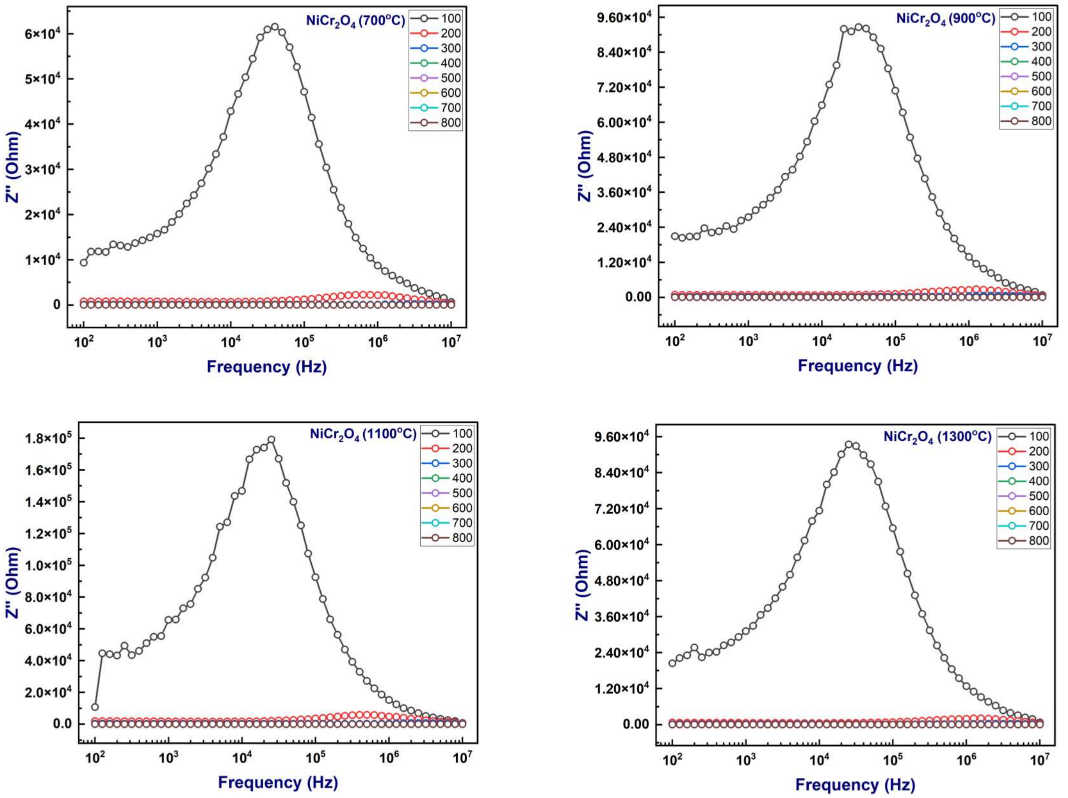

Figure 12. Variation of imaginary part of impedance of nickel chromite calcinated at 700, 900, 1100 and 1300°C with frequency in the temperature range 100-800°C.

hopping is shown by the peak frequencies, sometimes referred to as relaxation frequencies, which rise with temperature [54–56]. Non-Debye behavior is indicated by the broad breadth of the distribution of relaxation durations and the frequencies of relaxation peaks [57]. When the frequency of the applied electric field and the hopping frequency of localized electrons match, Debye peaks are seen. The discovery of relaxation peaks at low frequencies in the Z″ component of complex impedance is explained by space charge relaxation, which is linked to charge carriers from oxygen vacancies. It has long been known that space charge polarization predominates in materials with grains and grain boundaries. Debye peaks shift to higher frequencies as a result of the observed rise in electron hopping rate with temperature. Additionally, as the sample's resistive component releases less heat, Z″ drops with temperature. The change in Z″ as a function of temperature is shown in Figure 13 for a few chosen frequency ranges, ranging from 100 Hz to 10 MHz. At some frequencies, the observed Z″ decreases as the temperature increases. At certain frequencies, the energy of electrons exceeding the barrier potential for hopping may be the cause of the decrease in both the real and imaginary components of impedance with increasing temperature [58]. For samples sintered at 700, 900, 1100, and 1300°C, Figure 14 displays the Nyquist plots (Z′ vs. Z″) at room temperature. This helps us better understand how relaxation works. This supported the non-Debye type relaxation in NiCr$_2$O$_4$ since the semicircles were truncated in the center, and their centroid was situated below the true *Z*′ axis. Electric dipoles do not all relax at the same time during this procedure. Grain boundaries may contribute to this by direct current conduction [59,60]. This supports the case for an electrical process that depends just on relaxation qualities. The semicircle diameter in Nyquist plots indicates the contribution of grain boundaries, which is attributed to the resistance observed in the sintered samples [61]. The arc semicircles exhibit shifts

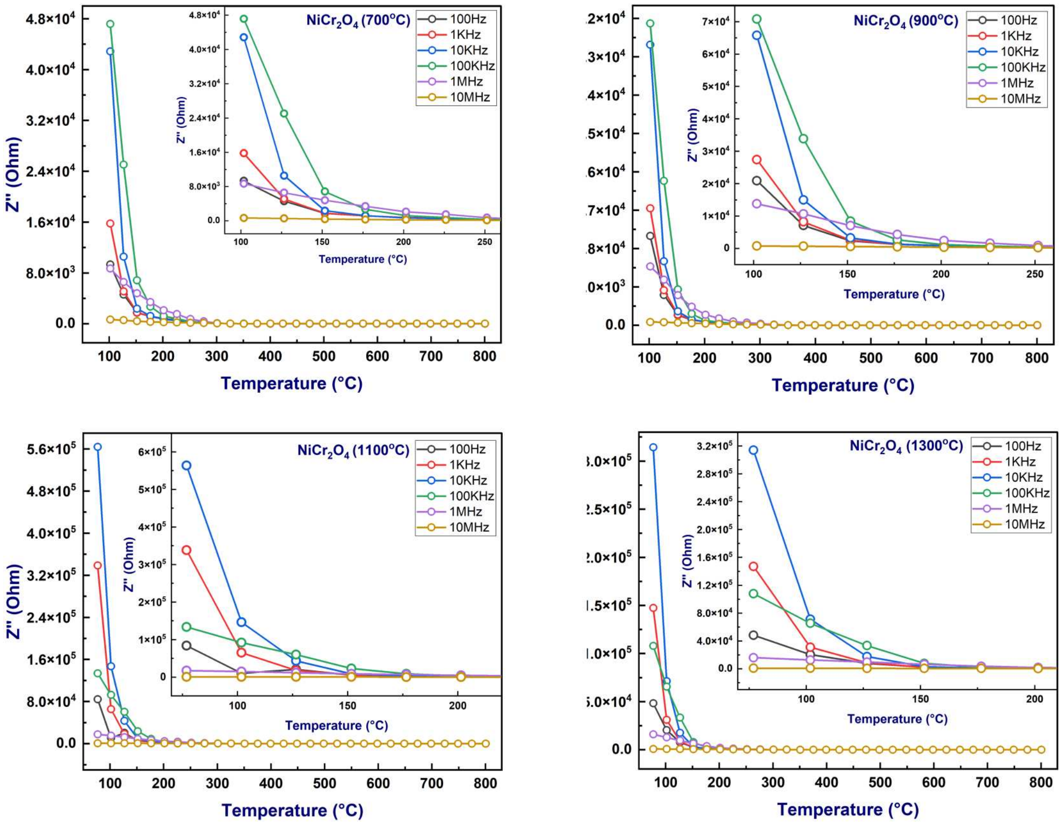

Figure 13. Variation of imaginary part of impedance of nickel chromite calcinated at 700, 900, 1100 and 1300°C with temperature at 100 Hz, 1kHz, 10kHz, 100kHz, 1 and 10 MHz.

corresponding to changes in the sintering temperature, which subsequently indicate variations in DC conductivity. Consequently, it is possible to calculate the capacitive and resistive characteristics of the prepared samples by considering relaxation and conduction in relation to the response of

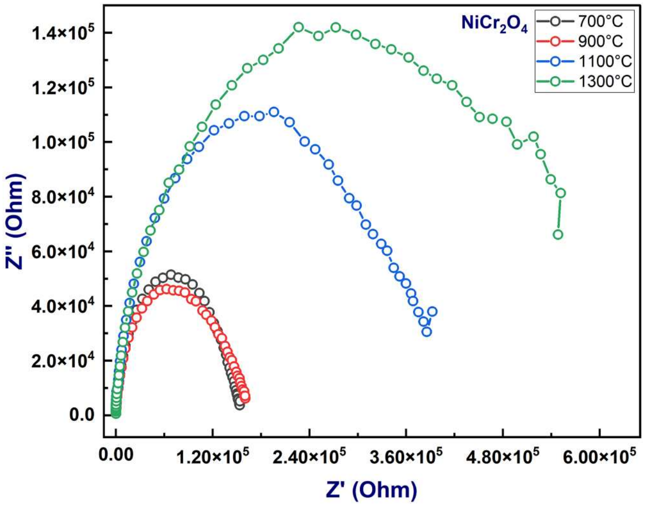

Figure 14. Cole-Cole plots of nickel chromite calcinated at 700, 900, 1100 and 1300°C with frequency at room temperature.

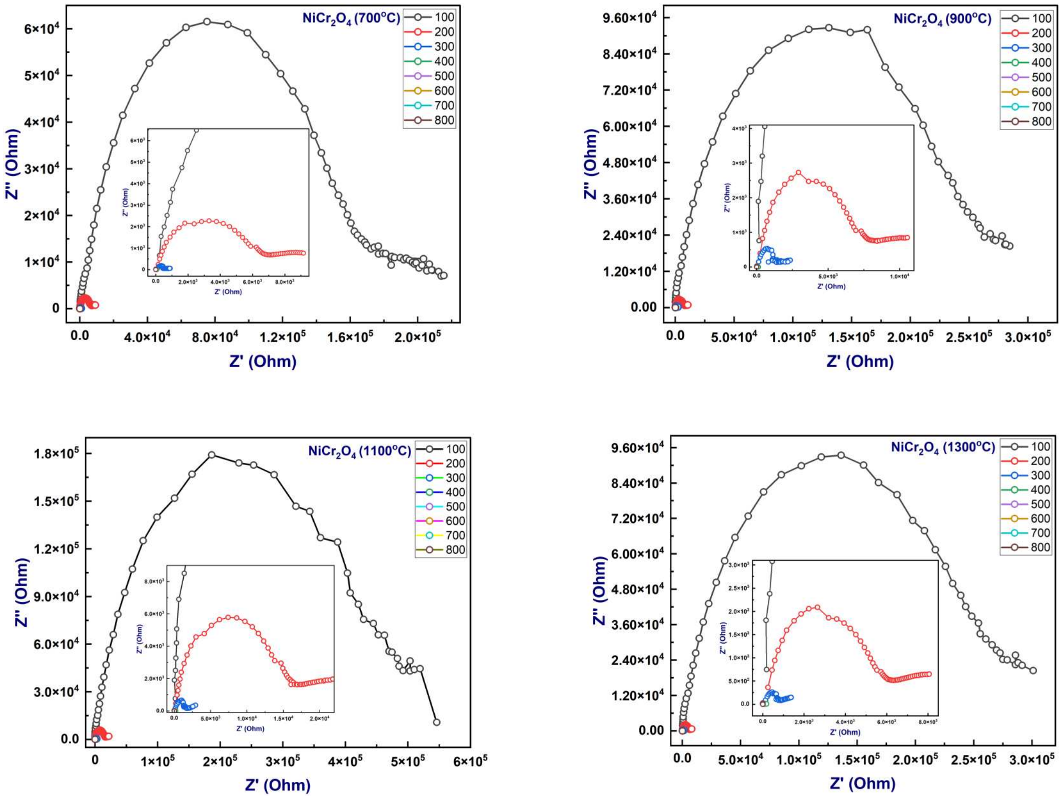

Figure 15. Cole-Cole plots of nickel chromite calcinated at 700, 900, 1100 and 1300°C with frequency in the temperature range 100-800°C.

grain boundary [50]. The plots illustrate both the low-frequency representation of the grain border region and the high-frequency representation of the grain region. The Nyquist plots (Z′ vs. Z″) as function of temperature for the synthesized samples, spanning from 100 to 800°C, are presented in Figure 15. $\sigma_{ac} = 2\pi f \varepsilon_r \tan\delta$ is the formula to compute the A.C., where f is the frequency of the applied electric field, tanδ is the media's dielectric loss tangent, and ε_r is the medium's dielectric constant. To obtain this formula, the double layer model is used, which takes into consideration the heterogeneous characteristics of two different layers [28], how often alternating current occurs. All prepared samples at room temperature have different conductivities (σ_{ac}), as shown in Figure 16. With increasing frequency conductivity rises. Enhanced charge carrier hopping, on the other hand, causes reduced resistance and improved conductivity at higher applied field frequencies [62]. Relatively a poor conducting thin layer of material is often observed in spinel materials, with the initial layer comprising course-grains of effectively conducting material [63]. The grain boundaries of nanomaterials play a crucial role in their transport properties due to the increased intensity of atoms at the edges or within a few layers of atoms. [64,65] The interchange of electrons among the similar ions in varying valence states leads to a phenomenon referred to as electron hopping, which is responsible for the electrical conductivity of nickel chromite [66,67]. While conductivity appears to be temperature independent at higher temperatures, it is discovered to be frequency dependent at lower temperatures (Figure 18). The pumping force of the applied frequency causes the conductivity to increase with frequency, aiding in the movement of charge carriers between various localized states and the release of trapped charges from various trapping locations. A substantial lattice vibration brought on by rising temperatures in the high temperature region scatters charge carriers and eliminates the frequency effect [68]. The current system enables

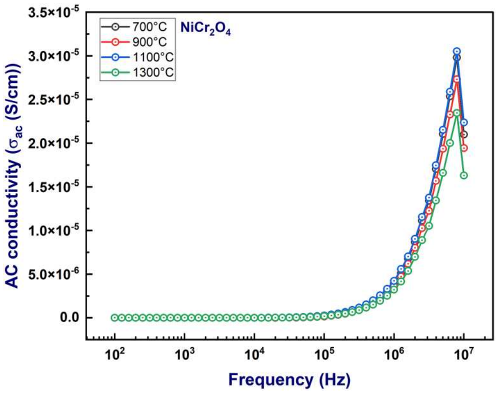

Figure 16. Variation of AC conductivity of nickel chromite calcinated at 700, 900, 1100 and 1300°C with frequency at room temperature.

conduction through the interchange of electrons in between Cr^{2+} and Cr^{3+} ions located at their octahedral sites. Figure 17 illustrates the AC conductivity of the synthesized materials across a temperature range of 100 to 800°C. From the Figure 17 it is clear that, for low frequencies (10^2 Hz to 10^4 Hz) show weak conductance dependency on frequency, and temperature. It could be due to According to the Maxwell-Wegner two-layer model, ferrites consist of well-conducting

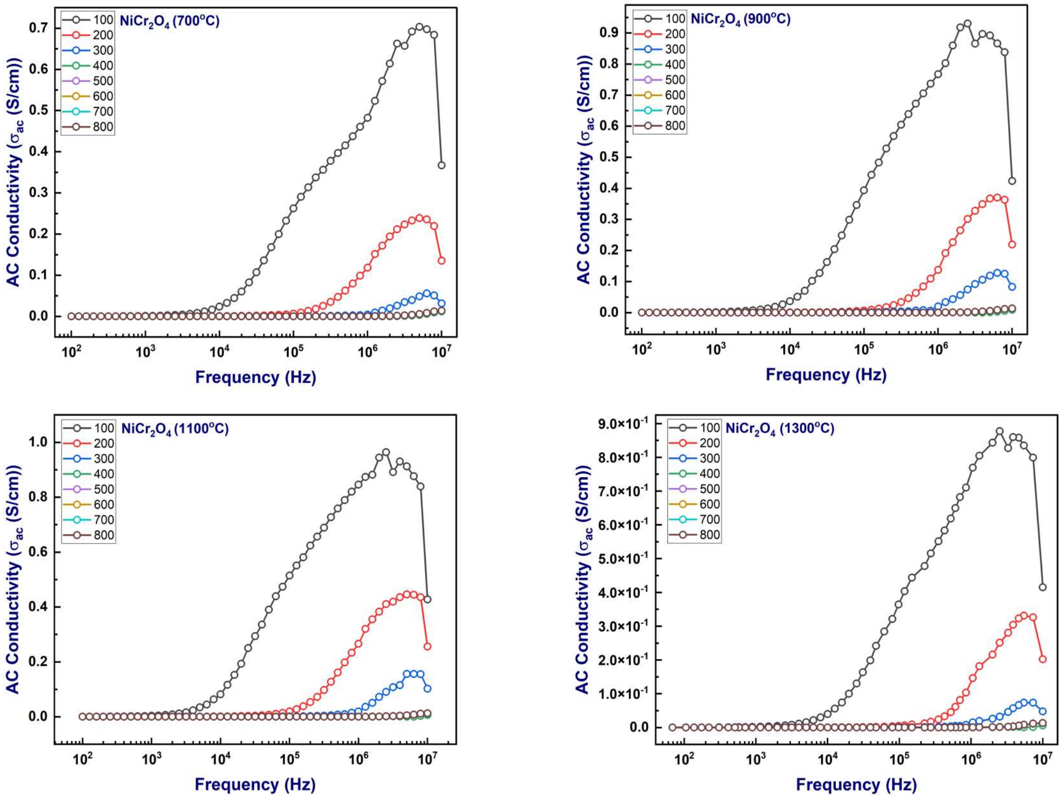

Figure 17. Variation of AC conductivity of nickel chromite calcinated at 700, 900, 1100 and 1300°C with frequency at temperature ranges from 100-800°C.

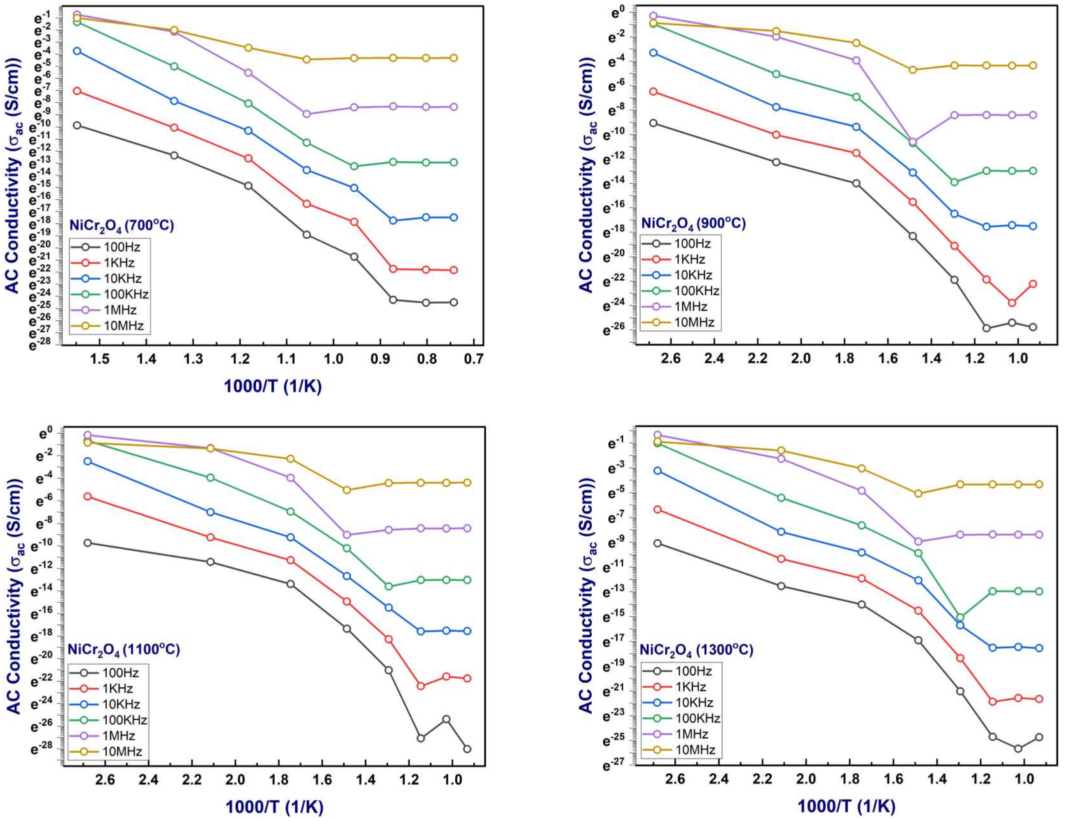

Figure 18. Variation of AC conductivity of nickel chromite calcinated at 700, 900, 1100 and 1300°C with temperature at 100 Hz, 1kHz, 10kHz, 100kHz, 1 and 10 MHz.

grains and poorly conducting grain borders that are more active at lower frequencies. Low conductance results from weak electron hopping in the area. At higher frequencies (>10^4 Hz) the conductivity shows increasing trend as the frequency increases, and exhibits decreasing trend as the temperature changes from 100 to 800°C. This significant increase of conductance with rising frequency can be described by the power law [69,70]. The conductivity of nickel chromite at temperatures of 700, 900, 1100, and 1300°C across various frequencies is illustrated in Figure 18. The findings indicated that as the frequency increased, the conductivity values exhibited a decrease. The sample could exhibit a more compact microstructure compared to other samples, potentially leading to a higher quantity of conduction species within the material. The conductivity of grain provides insights into the various types of polarons and the underlying conduction mechanisms. Grain activity is observed to rise at elevated frequencies; however, limitations on grain become evident at reduced frequencies. At low applied frequencies, a considerable accumulation of electronic charges at the grain border and decreased electron hopping between Cr^{2+} and Cr^{3+} cations result in reduced conductivity. However, due to grain conductivity and an increase in polaron hopping, conductivity gradually increases as frequency increases [71,72].

4. Conclusions

The synthesis of nickel chromite, represented by the chemical formula $NiCr_2O_4$, was achieved through sol–gel auto-combustion, followed by sintering at temperatures of 700, 900, 1100, and 1300°C. The X-ray diffractometry results were assessed at ambient temperature through the

Rietveld refinement technique to ascertain the phase purity of the material. Characteristics related to electricity include tangent loss, dielectric constant, and alternating current. The conductivity has been analyzed using the LCR meter. The variations in dielectric parameter, impedance, and A.C. conductivity was examined at room temperature and within the temperature range of 100–800° C, across frequencies from 100 Hz to 10 MHz. The investigation revealed that both temperature and frequency contributed to the improvement of the dielectric characteristics. The limited conductivity of the samples can be explained by the restricted electron hopping between the Cr^{2+} and Cr^{3+} cations as a result. The Maxwell–Wagner interfacial polarization provides substantial support for these findings. The examination indicated that the dielectric properties of the produced chromites could be enhanced, suggesting that they are promising candidates for notable physical attributes after assessing various concentrations. The selected material candidates exhibit significant benefits for high-frequency and microwave applications.

Disclosure statement

No potential conflict of interest was reported by the author(s).

References

[1] Kocsis V, Bordacs S, Varjas D, et al. Magnetoelasticity in *A*Cr2O4 spinel oxides (*A*= Mn, Fe, Co, Ni, and Cu). Phys Rev B. 2001;87:064416. doi:10.1103/PhysRevB.87.064416

[2] Maignan A, Martin C, Singh K, et al. From spin induced ferroelectricity to dipolar glasses: spinel chromites and mixed delafossites. J Solid State Chem. 2012;195:41–49. doi:10.1016/j.jssc.2012.01.063

[3] Singh K, Maignan A, Simon C, et al. $Fecr_2o_4$ and $CoCr_2O_4$ spinels: multiferroicity in the collinear magnetic state. Appl Phys Lett. 2011;99:172903. doi:10.1063/1.3656711

[4] Aslam S, Shifa MS, Gilani ZA, et al. Structural, optical and magnetic elucidation of co-doping of Nd^{3+} and Pr^{3+} on lithium nanoferrite and its technological application. Res Phys. 2019;12:1334–1339. doi:10.1016/j.rinp.2019.01.018.

[5] Tomiyasu K, Kagomiya I. Magnetic structure of $NiCr_2O_4$ studied by neutron scattering and magnetization measurements. J Phys Soc. 2004;73:2539–2542. doi:10.1143/JPSJ.73.2539

[6] Ohgushi K, Okimoto Y, Ogasawara T, et al. Magnetic, optical, and magnetooptical properties of Spinel-Type ACr_2X_4 (A=Mn, Fe, Co, Cu, Zn, Cd; X=O, S, Se). J Phys Soc. 2008;77:034713. doi:10.1143/JPSJ.77.034713.

[7] Khelifi J, Nasri M, Dhahri E. Investigation of the critical magnetic properties in $La_{0.6}Sr_{0.4}Mn_{0.9}V_{0.1}O_3$ manganite oxide. J Supercond Nov Magn. 2016;29:753–758. doi:10.1007/s10948-016-3575-2

[8] Yamasaki Y, Miyasaka S, Kaneko Y, et al. Magnetic reversal of the ferroelectric polarization in a multiferroic spinel oxide. Phys Rev Lett. 2006;96:207204. doi:10.1103/PhysRevLett.96.207204

[9] Dey K, Majumdar S, Giri S. Ferroelectricity in spiral short-range-ordered magnetic state of spinel $MnCr_2O_4$: significance of topological frustration and magnetoelastic coupling. Phys Rev B. 2014;90:184424. doi:10.1103/PhysRevB.90.184424.

[10] Gilani ZA, Shifa MS, Noor ul Huda Khan Asghar HM, et al. New $LiCo_{0.5}Pr_xFe_{2-x}O_4$ nanoferrites: prepared via low cost technique for high density storage application. J CeramInt. 2018;44(2):1881–1885. doi:10.1016/j.ceramint.2017.10.126

[11] Mandal PR, Singh R, Das A, et al. Enhanced magnetodielectric response in Dy modified $NiCr_2O_4$. J Magn Magn Mater. 2017;432:49–55. doi:10.1016/j.jmmm.2017.01.090

[12] Kumar R, Upadhyay SK, Xiao Y, et al. Influence of Fe substitution on multiferrocity and magneto-dielectric properties in $CoCr_2O_4$. J Phys D Appl Phys. 2018;51:385001. doi:10.1088/1361-6463/aad753

[13] Devi Chandrasekhar K, Krishna Murthy J, Lin JY, et al. Magnetostructural coupling and multiferroic properties in the spin-frustrated system Ni1-xZnxCr2O4. Phys RevB. 2016;94:205143. doi:10.1103/PhysRevB.94.205143

[14] Zhu CM, Yu GB, Wang LG, et al. Dielectric relaxation and magnetodielectric effect in the spinel $NiCr_2O_4$. J Magn Magn Mater. 2020;506:166803. doi:10.1016/j.jmmm.2020.166803

[15] Klemme S, van Miltenburg JC. Thermodynamic properties of nickel chromite ($NiCr_2O_4$) based on adiabatic calorimetry at low temperatures. Phys Chem Miner. 2002;29:663–667. doi:10.1007/s00269-002-0280-4

[16] Khelifi J, Tozri A, Dhahri E. Influence of quenched disorder on the structural properties and spin-wave excitations in ferromagnetic metallic manganites $(La_{1-x}Nd_x)_{2/3}(Ca_{1-y}Sr_y)_{1/3}MnO$. J Supercond Nov Magn. 2013;26:3133–3141. doi:10.1007/s10948-013-2131-6.

[17] Pandey GC, Nemkovski K, Su Y, et al. Evidence of anomalous conventional and spontaneous exchange bias, high coercivity in Fe doped $NiCr_2O_4$ spinel. Dalton Trans. 2020;49:4502–4517. DOI: https://doi.org/10.1039D0DT00124D.

[18] Orlandi MO, Ramirez MA, Foschini CR, et al. Giant dielectric constant materials and their applications. In: Aparicio M, Jitianu A, Klein L, editors. Sol-Gel processing for conventional and alternative energy. advances in Sol-Gel derived materials and technologies. Boston, MA: Springer; 2012. p. 123–146. doi:10.1007/978-1-4614-1957-0_7

[19] Souifi K, Nasri M, Hcini S, et al. Synthesis, structural and magnetic behavior and theoretical approach to study the magnetic and magnetocaloric properties of the half-doped perovskite $Nd_{0.5}Ba_{0.5}CoO_3$. J Mater Sci: Mater Electron. 2021;32:15291–15306. doi:10.1007/s10854-021-06079-y

[20] Sadashivappa PK, Venkatachalam R, Pothu R, et al. Progressive review of functional nanomaterials-based polymer nanocomposites for efficient EMI shielding. N J Compos Sci. 2023;7:77. doi:10.3390/jcs7020077

[21] Banerjee P, Franco A, Jr. Rare earth and transition metal doped $BiFeO_3$ ceramics: structural, magnetic and dielectric characterization. J Mater Sci Mater Electron. 2016;27:6053–6059. doi:10.1007/s10854-016-4530-5.

[22] Kumar KV, Bhavani SD. Influence of calcination temperature on physical and optical properties of nickel chromite nanoparticles. Sci Sinter. 2022;54(4):457. doi:10.2298/SOS2204457K

[23] Ragupathi C, Vijaya JJ, Kennedy LJ. Synthesis, characterization of nickel aluminate nanoparticles by microwave combustion method and their catalytic properties. MatSciEngB. 2014;184:18. doi:10.1016/j.mseb.2014.01.010

[24] Kumar KV, Bhavani SD. Effect of calcination temperature on structural and optical properties of nickel aluminate nanoparticles. East Eur J Phys. 2023;3:355. doi:10.26565/2312-4334-2023-3-37

[25] Javed M, Khan AA, Kazmi J, et al. Dielectric relaxation and small polaron hopping transport in sol-gel-derived $NiCr_2O_4$ spinel chromite. J Mater Res Bull. 2021;138:111242. doi:10.1016/j.materresbull.2021.111242

[26] Maxwell JC. Electricity and magnetism. London: Oxford University Press; 1873. 1 328.

[27] Wagner KW. Zur Theorie der Unvollkommenen Dielektrika. Ann Phys. 1913;40:817. doi:10.1002/andp.19133450502

[28] Koops CG. On the dispersion of resistivity and dielectric constant of some semiconductors at audio frequencies. Phys Rev. 1951;83:121. doi:10.1103/PhysRev.83.121

[29] Van Uitert LG. Dc resistivity in the nickel and nickel zinc ferrite system. J Chem Phys. 1955;23(10):1883–1887. doi:10.1063/1.1740598

[30] Padmaraj O, Venkateswarlu M, Satyanarayana N. Structural, electrical and dielectric properties of spinel type $MgAl_2O_4$ nanocrystalline ceramic particles synthesized by the gel-combustion method. Ceram Int. 2015;1:3178. doi:10.1016/j.ceramint.2014.10.169

[31] Younis M, Saleem M, Atiq S, et al. Magnetic phase transition and magneto-dielectric analysis of spinel chromites: MCr_2O_4 (M = Fe, Co and Ni). CeramInt. 2018;44(9):10229–10235. doi:10.1016/j.ceramint.2018.03.024

[32] Kuru TŞ. Effect of calcination temperature on structural, magnetic, and dielectric properties of $Mg_{0.75}Zn_{0.25}Al_{0.2}Fe_{1.8}O_4$ ferrites. J Mater Sci: Mater Electron. 2024;35:415. doi:10.1007/s10854-024-12185-4.

[33] Barik SK, Choudhary RNP, Mahapatra PK. Impedance spectroscopy study of $Na_{1/2}Sm_{1/2}TiO_3$ ceramic. Appl Phys A. 2007;88:217. doi:10.1007/s00339-007-3990-0

[34] Kumar A, Singh BP, Choudhary RNP, et al. Characterization of electrical properties of Pb-modified $BaSnO_3$ using impedance spectroscopy. Mat Chem Phys. 2006;99:150. doi:10.1016/j.matchemphys.2005.09.086.

[35] Benatia A, Gouitaa N, Lamcharfi T-d, et al. Effect of calcination temperature and duration on structural and dielectric properties of $CaFeO_{3-\delta}$. Arab J Chemens. 2024;17:105407. doi:10.1016/j.arabjc.2023.105407

[36] Souifi K, Rejaiba O, Nasri M. Hopping conduction mechanism and impedance spectroscopy analyses of the half-doped perovsikte $Nd_{0.5}Ba_{0.5}FeO_3$ prepared by sol–gel method. Appl Phys A. 2022;128:981. doi:10.1007/s00339-022-06131-6

[37] Godara S, Sinhaa N, Ray G. et al. Combined structural, electrical, magnetic and optical characterization of bismuth ferrite nanoparticles synthesized by auto-combustion route. J Asian Ceram Soc. 2014;2:416–421. doi:10.10.16/j.jascer.2014.09.001

[38] Venkatesh R, Pratibha S, Dhananjaya N, et al. Study of optical and dielectric properties of alkali metal cation (Li^+, Na^+, K^+) co-doped Eu^{3+} activated gadolinium aluminate nanoparticles. Mater Res Express. 2019;6:095008. doi:10.1088/2053-1591/ab268b

[39] Nasri M, Rejaiba O, Charguia R. Temperature and frequency dependence of negative capacitance, dielectric and electric properties in $La_{0.57}Nd_{0.1}Sr_{0.13}Ag_{0.2}MnO_3$ ceramic. J LowTemp Phys. 2022;206:250–268. doi:10.1007/s10909-021-02656-x

[40] Mazen SA, Dawoud HA. Temperature and composition dependence of dielectric properties in Li–Cu ferrite, J.Mat. Chem Phys. 2003;82:557–566. doi:10.1016/S0254-0584(03)00200-1

[41] Das PR, Biswal L, Behera B, et al. Structural and electrical properties of $Na_2Pb_2Eu_2W_2Ti_4X_4O_{30}$ (X = Nb, Ta) ferroelectric ceramics. J Mat Res Bull. 2009;44(6):1214–1218. doi:10.1016/j.materresbull.2009.01.013

[42] Mallick P, Uday Naik A, Mohanty D, et al. Synthesis and analysis of structural, dielectric, and thermistor behaviour of zinc ferrite. J Chem Phys Impact. 2023;6:100217. doi:10.1016/j.chphi.2023.100217

[43] SibyKurien SS, Mathew J, George KC. Structural and electrical properties of nano-sized magnesium aluminate. Indian JPure & App Phys. 2004;42(12):926.

[44] Bhavani SD, Purna Chandra Rao B, Kumar KV, et al. Synthesis and characterization of structural properties—RT and temperature-dependent dielectric behavior of Gd-substituted nickel nanoferrites. J Mater Sci: Mater Electron. 2024;35:1483. doi:10.1007/s10854-024-13248-2

[45] Rayssi C, Kossi SE, Dhahri J, et al. Frequency and temperature-dependence of dielectric permittivity and electric modulus studies of the solid solution $Ca_{0.85}Er_{0.1}Ti_{1-x}Co_{4x/3}O_3$ ($0\leq x\leq 0.1$). RSC Adv. 2018;8:17139. doi:10.1039/c8ra00794b

[46] Mandal SK, Singh S, Dey P, et al. Frequency and temperature dependence of dielectric and electrical properties of TFe_2O_4 (T=Ni, Zn, $Zn_{0.5}Ni_{0.5}$) ferrite nanocrystals. J Alloys Compd. 2016;656:887–896. doi:10.1016/j.jallcom.2015.10.045

[47] Sinclair D. Characterization of electro-materials using ac impedance spectroscopy. Bol Soc Esp Ceram Vidrio. 1995;34(2):55.

[48] Costa M, Pires GFM, Terezo A, et al. Impedance and modulus studies of magnetic ceramic oxide $Ba_2Co_2Fe_{12}O_{22}(Co_2Y)$ doped with Bi_2O_3. J Appl Phys. 2011;110(3):034107. doi:10.1063/1.3615935

[49] Kour S, Mahajan H, Mukherjee R. Influence of sintering temperature on impedance and modulus spectroscopy of nickel-substituted cobalt ferrite. J Mater Sci: Mater Electron. 2023;34:594. doi:10.1007/s10854-023-10030-8

[50] Karmakar S, Behera D. Non-overlapping small polaron tunnelling conduction coupled dielectric relaxation in weak ferromagnetic $NiAl_2O_4$. J Phys: Condens Matter. 2019;31:245701. doi:10.1088/1361-648X/ab03f0

[51] Dhibi H, Rejaiba O, Khelifi J, et al. Comprehensive investigation of structural, morphologic, optical, dielectric and electrical of $Ni_{0.3}Cd_{0.7}Cr_2O_4$ chromite to optoelectronic application. J Inorg Org Metal Poly Mat. 2023;33:3984. doi:10.1007/s10904-023-02703-y

[52] Hajlaoui ME, Gharbi S, Dhahri E, et al. Impedance spectroscopy and giant permittivity study of $ZnFe_2O_4$ spinel ferrite as a function of frequency and temperature. J Alloys Compd. 2022;906:164361. doi:10.1016/j.jallcom.2022.164361

[53] Das R, Sarkar T, Mandal K. Multiferroic properties of Ba^{2+} and Gd^{3+} co-doped bismuth ferrite: magnetic, ferroelectric and impedance spectroscopic analysis. J Phys D: Appl Phys. 2012;45:455002. doi:10.1088/0022-3727/45/45/455002

[54] Chen W, Zhu W, Tan OK, et al. Frequency and temperature dependent impedance spectroscopy of cobalt ferrite composite thick films. J Appl Phys. 2010;108:034101. doi:10.1063/1.3457217

[55] Karmakar S, Varma S, Behera D. Investigation of structural and electrical transport properties of nano-flower shaped $NiCo_2O_4$ supercapacitor electrode materials. J Alloys Comp. 2018;757:49. doi:10.1016/j.jallcom.2018.05.056

[56] Bharathi K, Markandeyulu G, Ramana CV. Impedance spectroscopic characterization of Sm and Ho doped Ni ferrites. J Electrochem Soc. 2011;158(3):G71. doi:10.1149/1.3534800

[57] Mandal SK, Singh S, Dey P, et al. Temperature and frequency dependence of AC electrical properties of Zn and Ni doped $CoFe_2O_4$ nanocrystals. Phil Mag. 2017;97(19):1628. doi:10.1080/14786435.2017.1312021

[58] Manimuthu P, Jamal Ghousia Mariam MN, Murugaraj R, et al. Metal-like to insulator transition in $Lu_3Fe_5O_{12}$. Phys Lett A. 2014;378:1402–1406. doi:10.1016/j.physleta.2014.03.018

[59] Adam J, Kumar KV, Kumar NH. Er^{3+} ion-doped Mg-Zn nanoferrite: properties and applications in dielectric, magnetic, structural, and optical domains affected by calcination temperature. Inorg Chem Commun. 2024;167:112698. doi:10.1016/j.inoche.2024.112698

[60] Khadhraoui S, Triki A, Hcini S, et al. Variable-range-hopping conduction and dielectric relaxation in $Pr_{0.6}Sr_{0.4}Mn_{0.6}Ti_{0.4}O_{3\pm\delta}$ perovskite. J Magn Magn Mater. 2014;371:69. doi:10.1016/j.jmmm.2014.07.044

[61] Ghasemi A, RezaLoghman-Estarki M, Torkian S, et al. The microstructure and magnetic behavior of spark plasma sintered iron/nickel zinc ferrite nanocomposite synthesized by the complex sol-gel method. Compos B Eng. 2019;175:107179. doi:10.1016/j.compositesb.2019.107179

[62] Batoo KM, Kumar S, Lee CG. Study of ac impedance spectroscopy of Al doped $MnFe_{2-2x}Al_{2x}O_4$. J Alloys Compd. 2009;480:596. doi:10.1016/j.jallcom.2009.01.137

[63] El hiti MA. Dielectric behavior and ac electrical conductivity of Zn-substituted Ni-Mg ferrites. J Magn Magn Mater. 1996;164:187. doi:10.1016/S0304-8853(96)00368-X

[64] Siegel WR. What do we really know about the atomic-scale structures of nanophase materials. J Phys Chem Solids. 1994;55(10):1097. doi:10.1016/0022-3697(94)90127-9

[65] Surya Narayana C. Structure and properties of nanocrystalline materials. Bull Mater Sci. 1994;17(4):307.

[66] Tabina Y, Withers RL. Cation ordering in $NiAl_2O_4$ spinel by a 111 systematic row CBED technique. Phys Chem Miner. 1999;27:112. doi:10.1007/s002690050247

[67] Kou L, Selman JR. Electrical conductivity and chemical diffusivity of $NiAl_2O_4$ spinel under internal reforming fuel cell conditions. J Appl Electrochem. 2000;30:1433. doi:10.1023/A:1026585124816

[68] Parveen A, Noorul Huda Khan Asghar HM, Khalid M, et al. Dielectric, impedance and modulus spectroscopic studies of $Co_{0.3}Cd_{0.7}Zn_{1.5x}Fe_{2-x}O_4$ nanoparticles. Appl Phys A. 2019;125:731. doi:10.1007/s00339-019-3029-3

[69] Atif M, Nadeem M. Sol–gel synthesis of nanocrystalline $Zn_{1-x}Ni_xFe_2O_4$ ceramics and its structural, magnetic and dielectric properties. J Sol-Gel Sci Technol. 2014;72:615–626. doi:10.1007/s10971-014-3484-4

[70] Sharma J, Parashar J, Saxena VK, et al. Study of dielectric properties of nanocrystalline cobalt ferrite upto microwave frequencies. Macromol Symp. 2015;357:38–42. doi:10.1002/masy.201400183

[71] Atif M, Idrees M, Nadeem M, et al. Investigation on the structural, dielectric and impedance analysis of manganese substituted cobalt ferrite i.e. Co 1− x Mn x Fe 2 O 4 (0.0≤ x≤ 0.4). RCS Adv. 2016;6:20876. doi:10.1039/C5RA20621A

[72] Velhal NB, Patil ND, Shelke AR, et al. Structural, dielectric and magnetic properties of nickel substituted cobalt ferrite nanoparticles: effect of nickel concentration. AIP Adv. 2015;5:097166. doi:10.1063/1.4931908